

Molecular simulation of the vapour–liquid phase coexistence of neon and argon using *ab initio* potentials

Patrick S. Vogt,^a Rail Liapine,^a Barbara Kirchner,^a Anthony J. Dyson,^a Hanspeter Huber,^{*a} Gianluca Marcelli^b and Richard J. Sadus^b

^a Institut für Physikalische Chemie der Universität Basel, Klingelbergstr. 80, CH-4056, Basel, Switzerland E-mail: hanspeter.huber@unibas.ch

^b Centre for Molecular Simulation and School of Information Technology, Swinburne University of Technology, PO Box 218, Hawthorn, Victoria, 3122, Australia

Received 5th October 2000, Accepted 31st January 2001

First published as an Advance Article on the web 2nd March 2001

Gibbs ensemble simulations using *ab initio* intermolecular potentials are reported for the vapour–liquid phase coexistence of neon and argon. For neon two different quantum chemical *ab initio* potentials of well-known quality are used to investigate the effect of the quality of pair interactions. In addition calculations are also reported for neon using a potential that includes three-body interactions. For argon, simulations are compared with results obtained from *NPH*-ensemble molecular dynamics simulations. It is found that the results of a perfect pair potential must occur outside the experimental temperature–density phase envelope. Therefore, if a perfect pair potential is used, many-body interactions and quantum effects must be considered to obtain good agreement with experiment.

I. Introduction

In previous decades quantum chemistry was mainly used to calculate properties of single molecules. In the 1970s and 1980s first combinations with simulations for the *ab initio* prediction of liquid properties appeared with the pioneering work of Clementi and coworkers on water^{1,2} and the Car–Parrinello method.³ In the last decade accurate quantitative calculations of simple real systems such as rare gases became feasible, and now also work on more complicated systems like carbon dioxide and water is increasing.^{4,5} We have investigated neon, applying two pair potentials (NE1⁶ and NE2⁷), obtained from quantum chemical calculations of different quality. Thermodynamic and transport properties were obtained quite accurately from the better pair potential (NE2), the pressure being the property most sensitive to approximations,⁸ which suggests that vapour–liquid phase coexistence might also be sensitive to these approximations. A further improvement was achieved by including an *ab initio* three-body potential NE3 in the simulation⁹ and accounting for quantum effects using a perturbational approach (NE2 WK) for the calculation of pair distribution functions.¹⁰ Similar although less work was performed on argon.^{10–12} These results represent a benchmark for the bulk properties of one-phase systems. It is of interest to determine whether the *ab initio* potentials can predict the properties of coexisting phases. In a first step the melting curves of neon¹³ and argon¹⁴ were calculated, showing that the pair potentials are able to reproduce the curves quite accurately between about 50 K and ambient temperatures. A more sensitive test however is the boiling curve which is the subject of this paper.

The melting curve was calculated by non-equilibrium molecular dynamics simulations in an *NPH*-ensemble (*i.e.* the number of particles N , the pressure P and the enthalpy H are kept constant) melting a non-ideal crystal. This approach is not convenient for the present case because of the expected effect of a large hysteresis.¹⁵ Hence we turned to Monte Carlo simulations in the Gibbs ensemble. Panagiotopoulos intro-

duced this method^{16,17} and it has been extended and developed further by several groups (see *e.g.* ref. 18–22, for a more thorough review see ref. 23). For argon a few points were calculated by molecular dynamics simulations in the *NPH*-ensemble, showing that the results from the Gibbs ensemble were within the hysteresis of molecular dynamics simulations. For neon the influences of the quality of the pair potential, of the three-body effects and of quantum effects are investigated.

Together with our previous work, this is part of an investigation on the significance of different contributions (quality of pair potential, many-body effects, translational quantum effects) for different bulk properties in an *ab initio* approach.

Similar investigations have been reported by Leonhard and Deiters²⁴ during the refereeing process of the present work. Instead of an *ab initio* three-body potential they combined an empirical Axilrod–Teller (AT) term with an *ab initio* pair potential.

II. Computational methods

Simulations were performed with the *NVT* Gibbs ensemble Monte–Carlo (GEMC) method.^{16,17} The program described in ref. 16 was modified to enable the implementation of any pair potential. This change concerned mainly the particle displacement and the volume change part.

A. Calculation with pair potentials

The system consists of two cubic boxes, with a constant total volume and periodic boundary conditions. One complete Monte Carlo cycle (MCC) contains three individual steps: first attempted displacements for all atoms, second an attempted volume change step and third an interchange attempt for 10% of all atoms.

The potential was truncated at a fixed value of 5σ for argon and 7σ for neon, respectively, where σ is the distance with a zero potential energy. To correct for the effect of this truncation long-range corrections were applied using the con-

ventional procedure as described elsewhere.¹⁵ To keep the cutoff radius smaller than half the box length during the whole simulation, *i.e.* when the size of the two individual boxes changes, a total of at least 1000 atoms for argon and 4000 atoms for neon had to be used. The large cutoff distances are discussed in Section III A.

The system was equilibrated until the pressure and the density in both boxes no longer showed a systematic drift, which typically took 40 000 MCC. Then two or three numerically independent simulations of 20 000 MCC were carried out as production runs.

For argon we performed in addition a few runs with a molecular dynamics program in an *NPH*-ensemble as described in ref. 14. These simulations result in a large hysteresis, but they are a good check for the correctness of the GEMC simulations, as they are performed in a completely independent way.

Potentials for argon and neon were obtained from quantum chemical *ab initio* calculations. A potential calculated by Woon²⁵ eqn. (1) was used for argon. For the neon simulations, we used two potentials of different quality from our group (NE1⁶ eqn. (2) and NE2⁷ eqn. (3)) and, a quantum effective Wigner–Kirkwood potential (NE2 WK¹⁰) based on NE2.

$$\frac{E_{\text{Woon}}(R)}{E_{\text{h}}} = \varepsilon \left(Q \exp \left(- \sqrt{\frac{(Q+1)k_{\text{e}}}{Q\varepsilon}} \left(\frac{R}{a_0} - R_{\text{e}} \right) \right) - (Q+1) \exp \left(- \sqrt{\frac{Qk_{\text{e}}}{(Q+1)\varepsilon}} \left(\frac{R}{a_0} - R_{\text{e}} \right) \right) \right) \quad (1)$$

where R is the intermolecular separation, E_{h} is the Hartree, a_0 is the Bohr radius, $\varepsilon = 0.4228 \times 10^{-3}$, $k_{\text{e}} = 0.6627 \times 10^{-3}$, $R_{\text{e}} = 7.1714$ and $Q = 0.6060$.

$$\frac{E_{\text{NE1}}(R)}{E_{\text{h}}} = a_1 \exp \left(- a_2 \frac{R}{a_0} \right) + a_3 \left(\frac{R}{a_0} \right)^{-12} + a_4 \left(\frac{R}{a_0} \right)^{-10} + a_5 \left(\frac{R}{a_0} \right)^{-8} + a_6 \left(\frac{R}{a_0} \right)^{-6} \quad (2)$$

where $a_1 = 1.48735474 \times 10^2$, $a_2 = 2.3520917$, $a_3 = 3.749754 \times 10^4$, $a_4 = 5.160348 \times 10^3$, $a_5 = 8.3724779$ and $a_6 = 6.8028878$.

$$\frac{E_{\text{NE2}}(R)}{E_{\text{h}}} = a_1 \exp \left(- a_2 \left(\frac{R}{a_0} \right)^2 \right) + a_3 \exp \left(- a_4 \left(\frac{R}{a_0} \right)^2 \right) + a_5 \exp \left(- a_6 \left(\frac{R}{a_0} \right)^2 \right) + a_7 \left(\frac{R}{a_0} \right)^{-10} + a_8 \left(\frac{R}{a_0} \right)^{-8} + a_9 \left(\frac{R}{a_0} \right)^{-6} \quad (3)$$

where $a_1 = 1.174594$, $a_2 = 0.355905$, $a_3 = 1.325805 \times 10^{-1}$, $a_4 = 0.214065$, $a_5 = 976.69318 \times 10^{-6}$, $a_6 = 0.105389$, $a_7 = 5.412694 \times 10^3$, $a_8 = -3.512808 \times 10^2$ and $a_9 = -3.964331$.

The accuracies of the NE1 and the NE2 potentials were well characterised in comparison with experimental pair properties^{6,7} like spectroscopic data and the second virial coefficients. In particular, this led to the conclusion that properties obtained with the NE2 potential deviate less or equally from experiment, than NE1 deviates from NE2 for that property.

The statistical errors were calculated as standard errors from batches of 100 MCC. We assumed this to be a reasonable length for the liquid state. For the vapour state, test calculations with different batch length showed that the data are correlated over roughly 1500 MCC, hence we multiplied the above errors for the vapour by a factor 4 (*i.e.* $\approx \sqrt{1500/100}$). The correlation of data appears to change with the phase points. Hence, the statistical errors might be larger in some states than the given values.

B. Calculations with the NE3 potential

In general, calculations for the vapour–liquid equilibria using the NE3 potential⁹ eqn. (4) followed the same procedure as outlined above. However, the increased computational requirement imposed by evaluating three-body interaction meant that the system size was restricted to 500 neon atoms, and hence a variable cutoff was applied. Typically 3000 MCC were used consisting of 500 attempted displacements, one attempted volume fluctuation and 500 interchange attempts were used. The system was equilibrated for 1500 MCC and averages were accumulated for a further 1500 MCC. For this system size, the number of successful interchanges increased considerably with increasing temperature. At higher temperatures, 10 exchange attempts per cycle were sufficient, 4500 MCC were used for equilibration and averages were accumulated for a further 4500 MCC.

$$E_{\text{NE3}}(R_{12}, R_{13}, R_{23}, \alpha_1, \alpha_2, \alpha_3) = E_{\text{NE1}}(R_{12}) + E_{\text{NE1}}(R_{13}) + E_{\text{NE1}}(R_{23}) + \Delta E_3$$

$$\frac{\Delta E_3}{E_{\text{h}}} = \frac{a_1}{\rho^4(1 + a_2\rho + a_3\rho^2)} + \frac{Q(a_4 + a_5\rho)}{\rho^4(1 + a_6\rho + a_7\rho^2)} + \frac{Q^2 a_8}{\rho^3}$$

$$\rho = \frac{R_{12}}{a_0} \times \frac{R_{13}}{a_0} \times \frac{R_{23}}{a_0}$$

$$Q = \cos(\alpha_1)\cos(\alpha_2)\cos(\alpha_3) \quad (4)$$

where R_{ij} is the intermolecular separation between atom i and j , α_i is the angle around atom i , $a_1 = -1494.04316399$, $a_2 = -2.40436522 \times 10^{-2}$, $a_3 = 1.98381726 \times 10^{-4}$, $a_4 = -3.34763381 \times 10^4$, $a_5 = 196.84364784$, $a_6 = -1.00003203 \times 10^{-2}$, $a_7 = 4.64397240 \times 10^{-5}$ and $a_8 = -77.45577385$.

III. Results and discussion

A. Cutoff radius and number of particles

The pressure of a liquid shows a very strong dependence on density and it is very sensitive to the shape of the potential. In GEMC simulations the two boxes should have the same pressure, when equilibrated. Hence, fine differences in the density of the liquid and vapour state, *e.g.* due to a different effect of a given cutoff radius in the two phases, can lead to large differences in pressure. Table 1 shows densities ρ and pressures P for the liquid and vapour states as a function of the cutoff radius for argon. In addition the dependence of the pressure difference together with its standard errors, obtained from 25 independent batches, each 100 MCC long, are shown. These results and similar investigations for neon lead us to choose the large cutoff radius of 5σ and 7σ for argon and neon, respectively. A similar sensitivity to the cutoff radius was observed for the surface tension by Mecke *et al.*²⁶

To obtain these desired cutoff values, the total number of particles had to be quite large, *i.e.* at least 1000 for argon and 4000 for neon. In most cases the number of particles in the two boxes were not extremely different. Hence, the problem pointed out by Valteau²⁷ that different particle numbers in the vapour and liquid phase might lead to strange boiling curves should be of minor importance here. Table 2 shows densities and pressures at a fixed cutoff radius of 2.5σ for different system sizes. The very small variation in pressure and density as a function of system size indicates that the system size is adequate.

B. Simulations with model potentials

Ab initio calculations of greater accuracy lead to an intermolecular potential with a deeper well and a smaller atomic-

Table 1 Dependence of density ρ , pressure P and pressure difference ΔP on cutoff radius for argon at $T = 125$ K (2000 particles, $\Delta P = P(\text{liquid}) - P(\text{vapour})$)

R_{cut}/σ	$\rho(\text{liquid})/\text{mol m}^{-3}$	$\rho(\text{vapour})/\text{mol m}^{-3}$	$P(\text{liquid})/\text{kPa}$	$P(\text{vapour})/\text{kPa}$	$\Delta P/\text{kPa}$
2.5	24 250 \pm 97	9818 \pm 219	4158 \pm 129	3580 \pm 182	578 \pm 145
3.0	23 629 \pm 127	5362 \pm 313	3370 \pm 112	3161 \pm 110	209 \pm 109
3.5	22 393 \pm 79	4814 \pm 340	3075 \pm 128	3032 \pm 147	43 \pm 108
4.5	22 952 \pm 81	5178 \pm 375	3113 \pm 118	3085 \pm 111	28 \pm 113
5.0	22 623 \pm 87	4823 \pm 248	3055 \pm 92	3063 \pm 146	-8 \pm 91

diameter.²⁸ To investigate the effect of this behaviour on GEMC simulation results, model calculations with a Lennard-Jones-[12,6]-potential (LJ) and various parameters ϵ and σ were performed. As only the trend was of interest these simulations were performed with a cutoff radius of 2.5σ and with a total particle number of 1000. After an equilibration of a few hundred steps, the mean over 40 000 MCC was taken. Results with parameters ϵ and σ typical for argon are shown in the Tables 3 and 4. These calculations show that in the temperature *vs.* density diagram an improved *ab initio* pair-potential will move the liquid (right) branch of the simulated curve towards, and finally, beyond the experimental one, whereas the change of the vapour (left) branch is harder to predict, but should be smaller. As will be seen below for the NE2 potential the simulated points are very close to the experimental curve. This is probably due to the fact that this is quite an accurate potential, but not yet exact, the latter would result in points outside the experimental curve.

C. Argon simulations

The results obtained for argon with the *ab initio* potential by Woon²⁵ are listed in Table 5 and the temperature *vs.* density graph is compared with experiment in Fig. 1. The simulated curve is, over the whole range, inside the experimental curve, in contrast to simulations with accurate empirical pair potentials.^{29,30} The reason for which is discussed in the model calculations in Section III B. The potential of Woon has a well-depth of 1.11 kJ mol⁻¹, whereas an accurate empirical estimate is 1.18 kJ mol⁻¹. The corresponding values for σ are

Table 2 Influence of the system size on the density and the pressure for argon at 125 K (cutoff radius 2.5σ)

Number of particles	$\rho(\text{liquid})/\text{mol m}^{-3}$	$\rho(\text{vapour})/\text{mol m}^{-3}$	$P(\text{liquid})/\text{kPa}$	$P(\text{vapour})/\text{kPa}$
1000	23 725 \pm 33	6610 \pm 115	4260 \pm 36	3409 \pm 30
1500	23 888 \pm 27	7200 \pm 108	4146 \pm 29	3464 \pm 21
2000	23 857 \pm 41	7858 \pm 52	4427 \pm 42	3484 \pm 42

Table 3 Change of orthobaric density ρ with potential depth ϵ for a LJ potential at 125 K ($\sigma = 335.2$ pm)

ϵ/K	$\epsilon/\text{kJ mol}^{-1}$	$\rho(\text{liquid})/\text{mol m}^{-3}$	$\rho(\text{vapour})/\text{mol m}^{-3}$
124	1.031	32 659 \pm 16	2851 \pm 68
129	1.073	33 371 \pm 16	1820 \pm 52
134	1.114	34 055 \pm 17	1398 \pm 32

Table 4 Change of orthobaric density ρ with atomic diameter σ for a LJ potential at 125 K ($\epsilon = 124$ K)

σ/pm	$\rho(\text{liquid})/\text{mol m}^{-3}$	$\rho(\text{vapour})/\text{mol m}^{-3}$
335	32 659 \pm 16	2851 \pm 68
350	28 623 \pm 11	2379 \pm 72
365	25 249 \pm 8	2253 \pm 84

379.5 pm and 376 pm, respectively. Using the values from the model calculations together with these numbers we estimate an increase in the liquid density by about 2000 mol m⁻³ and a decrease of the vapour density by about 1000 mol m⁻³. This confirms the expected shift of the temperature *vs.* density curve from the inside towards the outside of the experimental curve.

As described elsewhere,³¹ an estimate of the critical temperature and density can be obtained by fitting the simulation data to the critical exponent law ($\beta = 0.32$) and the law of rectilinear diameters. The critical pressure can be estimated by plotting the logarithm of pressure as a function of the inverse of temperature. This yields a critical temperature of 130.5 K compared to the experimental value of 150.7 K, a critical density of 13 190 mol m⁻³ compared to an experimental value of 13 410 mol m⁻³ and a critical pressure of 4.26 MPa compared to an experimental value of 4.91 MPa.

The points in Fig. 1 and 2 marked with *NPH* were obtained with an *NPH*-ensemble molecular dynamics program¹⁴ in non-equilibrium runs with a temperature gradient. The results compare favourably with the results from the GEMC simulations, but show large hysteresis. Starting at low temperature with a positive gradient, the boiling point was too high, whereas starting at high temperatures with a negative temperature led to condensation at too low temperatures. The

Table 5 GEMC simulations of argon

T/K	$\rho(\text{liquid})/\text{mol m}^{-3}$	$\rho(\text{vapour})/\text{mol m}^{-3}$	$P(\text{liquid})/\text{kPa}$	$P(\text{vapour})/\text{kPa}$
90	33 009 \pm 7	377 \pm 6	264 \pm 4	226 \pm 36
103	30 157 \pm 19	1101 \pm 16	778 \pm 70	804 \pm 10
111	28 164 \pm 17	1998 \pm 24	1392 \pm 44	1430 \pm 14
121	24 361 \pm 30	3849 \pm 100	2496 \pm 32	2524 \pm 40
125	21 749 \pm 34	5019 \pm 53	3201 \pm 21	3109 \pm 20

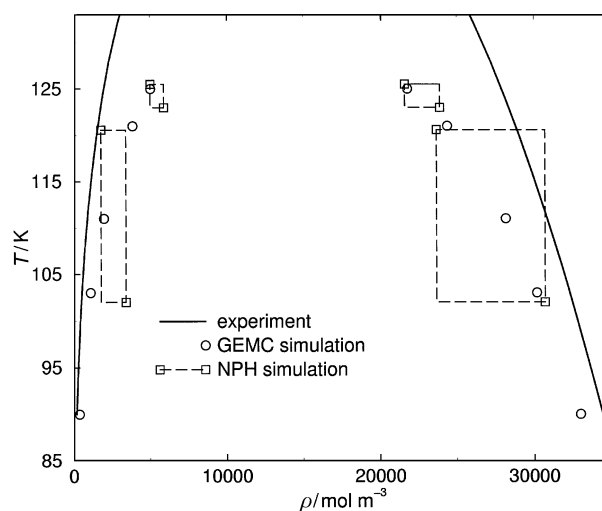


Fig. 1 Density ρ *vs.* temperature T for the liquid–vapour coexistence of argon. Experimental values from ref. 37.

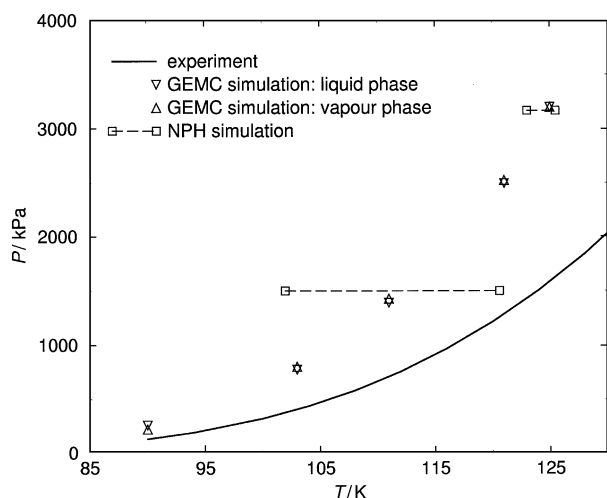


Fig. 2 Pressure P vs. temperature T for the liquid–vapour coexistence of argon. Experimental values from ref. 37.

results were also checked with some equilibrium runs in this region.

Fig. 2 shows pressure vs. temperature. As is also seen in Table 5 the pressure is reasonably well equilibrated and shows a good statistical accuracy. However, it deviates substantially from the experimental pressure. As work on neon with a three-body potential has shown,³² the inclusion of such interactions can change the pressure by a few MPa, hence the present deviations are not unexpected.

D. Neon simulations

In the case of neon we are able to study additional effects. The main results are obtained with the *ab initio* NE2 potential,⁷ which has been checked on experimental pair properties to be accurate to within a few percent. Comparing at two phase points with the less accurate NE1 potential,⁶ we can roughly predict the change we could expect with an exact pair potential. Another two simulations with the quantum effective Wigner–Kirkwood potential NE2 WK provides an indication of the expected changes due to quantum effects and, similarly, the inclusion of a three-body potential shows the influence of three-body interactions. Leonhard and Deiters²⁴ have used newer and slightly more accurate *ab initio* pair potentials than the ones used here for argon and neon. For the three-body interactions they use an AT term with empirical parameters from the literature, in contrast to our present work with an *ab initio* three-body potential. Their three-body interaction might be more accurate in the long-range part, whereas our potentials includes the short-range part, which was shown to be quite important.⁹ Leonhard and Deiters find that their potentials including the AT term yield good agreement with experiment especially for the vapour pressure. This is in contrast to our results, which show that the short-range part has quite an influence on the equilibrium. The solution to this contradiction is probably found in the analysis of Bukowski and Szalewicz,³³ who conclude that even though short-range contributions to the nonadditivity are quite large, cancellations occurring between these and other components at the interatomic distances typical for the liquid make the total three-body nonadditivity effect very similar to that given by a simple tripole–dipole potential.

1. NE2 potential. The results obtained for neon with the NE2 potential are listed in Table 6 and the temperature vs. density graph is compared with experiment in Fig. 3. The simulated curve is, over the whole range, inside but very close to the experimental one.

Table 6 GEMC simulations of neon with the NE2 potential

T/K	$\rho(\text{liquid})/\text{mol m}^{-3}$	$\rho(\text{vapour})/\text{mol m}^{-3}$	$P(\text{liquid})/\text{kPa}$	$P(\text{vapour})/\text{kPa}$
25	$62\,457 \pm 6$	228 ± 2	218 ± 12	46 ± 1
30	$56\,996 \pm 10$	1103 ± 6	375 ± 12	252 ± 1
32	$54\,734 \pm 13$	1708 ± 7	525 ± 9	397 ± 2
36	$49\,013 \pm 12$	3882 ± 34	962 ± 9	900 ± 6
40	$40\,610 \pm 24$	8539 ± 69	1776 ± 6	1767 ± 9

Fitting the data to the critical exponent law and the law of rectilinear diameters yields a critical temperature of 42.0 K compared to the experimental value of 44.4 K and a critical density of $23\,390 \text{ mol m}^{-3}$ compared to an experimental value of $23\,940 \text{ mol m}^{-3}$. The estimated critical pressure is 2.39 MPa compared to an experimental value of 2.65 MPa.

These relatively accurate results obtained with this potential are due to a fortuitous error cancellation as we will discuss below.

Even though the argon potential is, for many properties, of comparable quality to the NE2 potential, the resulting pressures deviate typically twice as much from the experimental pressures as the ones of NE2.¹¹ In this context it is not surprising that the argon GEMC simulations do not match the experimental data as well as the NE2 GEMC simulations, as the pressure is one of the quantities which influences the equilibration of the phases.

2. NE1, NE2 WK and NE3 potentials. Two phase points obtained with the less accurate NE1 potential are listed in Table 7 and compared graphically with the other results in Fig. 3. From the two points it is easily seen that the NE1 curve falls not only inside the experimental curve but also inside the NE2 curve. There is a small but distinct change for the vapour density and a quite large change for the liquid density.

From previous work⁷ we know that for the pressure the deviation of NE2 from experiment is about 2/3 of the deviation between NE1 and NE2. As at 30 and 32 K the NE2 points show good agreement with experiment we would assume that at these temperatures points from the exact pair potential would fall outside the curve by an amount about 2/3 of the deviation of the NE1 points from the experimental curve (see Fig. 3). Therefore, it can be inferred that the exact pair curve would clearly fall outside the experimental curve and the good agreement of the NE2 with the experimental curve must be due to error cancellation. This observation is

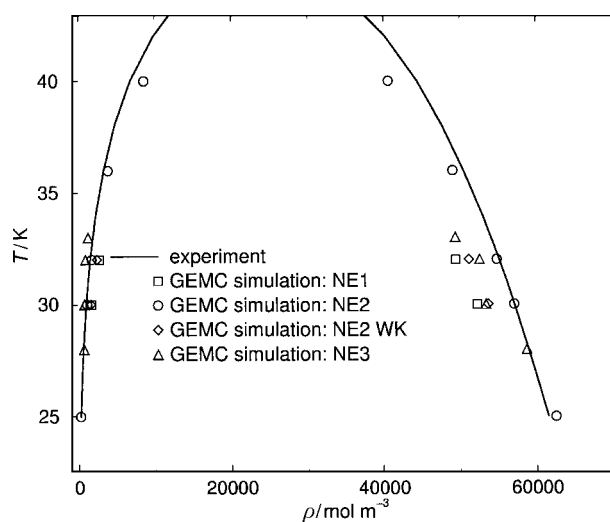


Fig. 3 Density ρ vs. temperature T for the liquid–vapour coexistence of neon. Experimental values from ref. 38.

Table 7 GEMC simulations of neon with the NE1, the NE2 WK and the NE3 potential

T/ K	$\rho(\text{liquid})/$ mol m^{-3}	$\rho(\text{vapour})/$ mol m^{-3}	P(liquid)/ kPa	P(vapour)/ kPa
NE1				
30	52 196 \pm 10	1711 \pm 4	548 \pm 10	372 \pm 1
32	49 386 \pm 14	2738 \pm 19	705 \pm 12	599 \pm 3
NE2 WK				
30	53 608 \pm 9	1598 \pm 6	440 \pm 7	349 \pm 1
32	51 111 \pm 13	2433 \pm 24	642 \pm 10	540 \pm 4
NE3				
28	58 681 \pm 449	686 \pm 84	—	—
30	53 332 \pm 563	770 \pm 27	—	—
32	52 497 \pm 836	902 \pm 17	—	—
33	49 357 \pm 1458	1245 \pm 87	—	—

consistent with earlier work on accurate empirical pair potentials. For example, Marcelli and Sadus³⁰ reported simulations of the phase behaviour exhibited by argon, krypton and xenon using accurate pair potentials such as the Barker–Fisher–Watts³⁴ potential. In all cases, accounting for only pair interactions resulted in a vapour–liquid coexistence curve that was outside of the experimental curve. However, when the additional contribution of three-body interactions was included, the liquid phase densities were predicted accurately. The *ab initio* calculations reported here support the hypothesis that pair interactions alone cannot be used to account for phase equilibria.

In the lower part of Table 7 we show the results at the same temperatures obtained with a quantum effective Wigner–Kirkwood potential NE2 WK based on the NE2 potential. As the potential in this case is temperature dependent there is no straightforward way to distinguish between kinetic and potential energy. This results in uncertainties in the calculation of pressure and the numerical results should only be considered as qualitatively accurate. Nonetheless, it is apparent (see also Fig. 3), that quantum effects would partially cancel the change due to an improved pair potential.

Calculations with the NE3 potential are summarised in Table 7 and compared with experiment in Fig. 3. Note that the results of these simulations have somewhat larger uncertainties due to the shorter runs and the smaller number of particles. We therefore omit the pressures in the table as they show quite large error bars. This potential is an NE2 pair potential which includes a contribution from three-body interactions and it is noticeable that the predicted densities fall slightly within the experimental phase envelope. This discrepancy with experiment can be attributed primarily to uncertainties in the representation of two-body interactions. Fitting the data to the critical exponent law and the law of rectilinear diameters yields a critical temperature of 44.7 K compared to the experimental value of 44.4 K and a critical density of 21 980 mol m⁻³ compared to an experimental value of 23 940 mol m⁻³. The inclusion of three-body interactions improves the agreement with experiment for temperature at the expense of a small reduction in the quality of the agreement for the critical density. A similar effect is observed³⁵ when the Lennard-Jones potential is combined with the Axilrod–Teller³⁶ term.

IV. Conclusion

GEMC simulations of the vapour–liquid coexistence curves for argon and neon are performed with potentials obtained from quantum chemical *ab initio* calculations. No empirical parameters are used in this study. In the temperature *vs.* density curve the pair potentials fall inside the experimental curves, *i.e.* the critical temperature is too small. But it is shown that improved quantum chemical calculations would yield

curves outside the experimental ones. Only by including translational quantum effects and many-body interactions the simulated curve brought back to the experimental one. This conclusion is consistent with work on accurate empirical pair potentials which indicates that pair interaction alone cannot account fully for vapour–liquid equilibria. In contrast to the empirical work the *ab initio* three-body potential applied here modifies the pair potential mainly in the repulsive area.

With the application of quantum chemical *ab initio* potentials in GEMC simulations, this work complements our previous work on bulk properties, where the significance of the quality of *ab initio* pair potentials, many-body interactions and translational quantum effects on different bulk properties were studied.

Acknowledgement

The authors gratefully acknowledge the Schweizerischer Nationalfonds zur Förderung der Wissenschaften (Project No. 20-058881.99) for financial support and the Swiss-HLR-Rat for a grant of computer time on the national supercomputer. Allocations of computer time on the Fujitsu VPP300 and NEC SX-5 computers were also provided by the Australian National University Supercomputing Centre and the CSIRO High Performance Computing and Communications Centre, respectively. GM thanks the Australian Government for an International Postgraduate Research Scholarship (IPRS).

References

- 1 G. C. Lie, E. Clementi and M. Yoshimine, *J. Chem. Phys.*, 1976, **64**, 2314.
- 2 O. Matsuoka, E. Clementi and M. Yoshimine, *J. Chem. Phys.*, 1976, **64**, 1351.
- 3 R. Car and M. Parrinello, *Phys. Rev. Lett.*, 1985, **55**, 2471.
- 4 H. Huber, A. Dyson and B. Kirchner, *Chem. Soc. Rev.*, 1999, **28**, 121.
- 5 U. K. Deiters, M. Hloucha and K. Leonhard, in *Chemistry for the 21st Century: Chemical Thermodynamics*, ed. T. M. Letcher, IUPAC Monograph Series, Blackwell, 1999, p. 187.
- 6 R. Eggenberger, S. Gerber, H. Huber and D. Searles, *Chem. Phys.*, 1991, **156**, 395.
- 7 R. Eggenberger, S. Gerber, H. Huber and M. Welker, *Mol. Phys.*, 1994, **82**, 689.
- 8 R. Eggenberger, H. Huber and M. Welker, *Chem. Phys.*, 1994, **187**, 317.
- 9 E. Ermakova, J. Solca, G. Steinebrunner and H. Huber, *Chem. Eur. J.*, 1998, **4**, 373.
- 10 E. Ermakova, J. Solca, H. Huber and D. Marx, *Chem. Phys. Lett.*, 1995, **246**, 204.
- 11 E. Ermakova, J. Solca, H. Huber and M. Welker, *J. Chem. Phys.*, 1995, **102**, 12; E. Ermakova, J. Solca, H. Huber and M. Welker, *J. Chem. Phys.*, 1995, **102**, 4942.
- 12 T. Pfeleiderer, I. Waldner, H. Bertagnolli, K. Tölheide, B. Kirchner, H. Huber and H. E. Fischer, *J. Chem. Phys.*, 1999, **111**, 2641.
- 13 J. Solca, A. J. Dyson, G. Steinebrunner, B. Kirchner and H. Huber, *J. Chem. Phys.*, 1998, **108**, 4107.
- 14 J. Solca, A. J. Dyson, G. Steinebrunner, B. Kirchner and H. Huber, *Chem. Phys.*, 1997, **224**, 253.
- 15 M. P. Allen and D. J. Tildesley, *Computer Simulations of Liquids*, Clarendon Press, Oxford, 1987.
- 16 A. Z. Panagiotopoulos, *Mol. Phys.*, 1987, **61**, 813.
- 17 A. Z. Panagiotopoulos, N. Quirke, M. Stapleton and D. J. Tildesley, *Mol. Phys.*, 1988, **63**, 527.
- 18 B. J. Palmer and C. Lo, *J. Chem. Phys.*, 1994, **101**, 10899.
- 19 T. Kristof and J. Liszi, *Chem. Phys. Lett.*, 1996, **261**, 620.
- 20 K. Kiyohara, T. Spyriouni, K. E. Gubbins and A. Z. Panagiotopoulos, *Mol. Phys.*, 1996, **89**, 965.
- 21 J. N. C. Lopes and D. J. Tildesley, *Mol. Phys.*, 1997, **92**, 187.
- 22 M. Strnad and I. Nezbeda, *Mol. Simul.*, 1999, **22**, 183.
- 23 R. J. Sadus, *Molecular Simulation of Fluids, Theory, Algorithms and Object-Oriented*, Elsevier, Amsterdam, 1999.
- 24 K. Leonhard and U. K. Deiters, *Mol. Phys.*, 2000, **98**, 1603.
- 25 D. E. Woon, *Chem. Phys. Lett.*, 1993, **204**, 29.
- 26 M. Mecke, J. Winkelmann and J. Fischer, *J. Chem. Phys.*, 1997, **107**, 9264.

- 27 J. P. Valleau, *J. Chem. Phys.*, 1998, **108**, 2962.
28 G. Gann, P. S. Vogt and H. Huber, *Chem. Phys.*, 2001, **263**, 333.
29 J. A. Anta, E. Lomba and M. Lombardero, *Phys. Rev. E*, 1997, **55**, 3; J. A. Anta, E. Lomba and M. Lombardero, *Phys. Rev. E*, 1997, **55**, 2707.
30 G. Marcelli and R. J. Sadus, *J. Chem. Phys.*, 1999, **111**, 4; G. Marcelli and R. J. Sadus, *J. Chem. Phys.*, 1999, **111**, 1533.
31 R. J. Sadus, *Mol. Phys.*, 1996, **87**, 897.
32 B. Kirchner, E. Ermakova, J. Solca and H. Huber, *Chem. Eur. J.*, 1998, **4**, 383.
33 R. Bukowski and K. Szalewicz, to be published.
34 J. A. Barker, R. A. Fisher and R. O. Watts, *Mol. Phys.*, 1971, **21**, 657.
35 R. J. Sadus, *Fluid Phase Equilib.*, 1998, **144**, 351.
36 B. M. Axilrod and E. Teller, *J. Chem. Phys.*, 1943, **11**, 299.
37 B. A. Younglove, *J. Phys. Chem. Ref. Data*, 1982, **11**, 1.
38 V. A. Rabinovich, A. A. Vasserman, V. I. Nedostup and L. S. Veksler, *Thermodynamic Properties of Neon, Argon, Krypton and Xenon*, Springer Verlag, Berlin, 1988.